THE JOURNAL OF BIOLOGICAL CHEMISTRY VOL. 289, NO. 40, pp. 27924–27936, October 3, 2014

The Atomic Resolution Structure of Human AlkB Homolog 7 (ALKBH7), a Key Protein for Programmed Necrosis and Fat Metabolism*[S]

Received for publication, June 19, 2014, and in revised form, July 31, 2014 Published, JBC Papers in Press, August 13, 2014, DOI 10.1074/jbc.M114.590505

Guoqiang Wang[‡], Qingzhong He[§], Chong Feng[‡], Yang Liu[‡], Zengqin Deng[‡], Xiaoxuan Qi[‡], Wei Wu[‡], Pinchao Mei[§], and Zhongzhou Chen[‡1]

From the [‡]State Key Laboratory of Agrobiotechnology, China Agricultural University, Beijing 100193 and the [§]Department of Biochemistry and Molecular Biology, National Key Laboratory of Medical Molecular Biology, Institute of Basic Medical Sciences, Chinese Academy of Medical Sciences and Peking Union Medical College, Beijing 100005, China

Background: Human ALKBH7 is a mitochondrial protein required for alkylation- and oxidation-induced programmed necrosis and short chain fatty acid metabolism.
Results: Atomic resolution structures of ALKBH7 in complex with two ligands were determined.
Conclusion: Structural analyses and observation of self-hydroxylation demonstrate that ALKBH7 may function as a protein hydroxylase.
Significance: ALKBH7 structures provide a foundation for drug design in cell death and metabolic diseases.

ALKBH7 is the mitochondrial AlkB family member that is required for alkylation- and oxidation-induced programmed necrosis. In contrast to the protective role of other AlkB family members after suffering alkylation-induced DNA damage, ALKBH7 triggers the collapse of mitochondrial membrane potential and promotes cell death. Moreover, genetic ablation of mouse Alkbh7 dramatically increases body weight and fat mass. Here, we present crystal structures of human ALKBH7 in complex with Mn(II) and α-ketoglutarate at 1.35 Å or *N*-oxalylglycine at 2.0 Å resolution. ALKBH7 possesses the conserved double-stranded β-helix fold that coordinates a catalytically active iron by a conserved H*X*(D/E) . . . X_n . . . H motif. Self-hydroxylation of Leu-110 was observed, indicating that ALKBH7 has the potential to catalyze hydroxylation of its substrate. Unlike other AlkB family members whose substrates are DNA or RNA, ALKBH7 is devoid of the "nucleotide recognition lid" which is essential for binding nucleobases, and thus exhibits a solvent-exposed active site; two loops between β-strands β6 and β7 and between β9 and β10 create a special outer wall of the minor β-sheet of the double-stranded β-helix and form a negatively charged groove. These distinct features suggest that ALKBH7 may act on protein substrate rather than nucleic acids. Taken together, our findings provide a structural basis for understanding the distinct function of ALKBH7 in the AlkB family and offer a foundation for drug design in treating cell death-related diseases and metabolic diseases.

Cell death, one of the most vital cellular responses of multicellular organisms, can be divided into apoptosis, autophagy, and necrosis based on different morphological appearance (1). Although apoptosis is well studied and regarded as programmed cell death, necrosis has been considered as an uncontrolled process that occurs as a result of infection or injury for a long time. However, the accumulating evidence reveals that necrosis is also well regulated as apoptosis in many cases. For example, the tumor necrosis factor (TNF)-induced programmed necrosis has unique signaling mechanisms mediated by receptor-interacting protein kinase 1 (RIP1) and RIP3. Programmed necrosis plays an important role in various pathological processes, including ischemic brain injury, neurodegenerative diseases, and viral infections (2). Necrosis-mediated via the poly(ADP-ribose) polymerase pathway is the other extensively studied model of programmed necrosis. In response to DNA damage caused by DNA-alkylating agents such as 1-methyl-3-nitro-1-nitrosoguanidine, the DNA repair enzyme poly(ADP-ribose) polymerase 1 is hyperactivated, resulting in massive depletion of nicotinamide adenine dinucleotide (NAD^+), dysfunction of mitochondria, abolishment of ATP production, and execution of programmed necrosis (3–5). Because many kinds of cancer cells are resistant to apoptosis, programmed necrosis emerges as an attractive target to activate the death of these cancer cells (6).

Recently, the mitochondrial protein human AlkB homolog 7 (ALKBH7) was found to be essential for alkylation- and oxidation-induced programmed necrosis, but it had no effect on apoptosis (7). ALKBH7-depleted cells were much more likely to survive than wild-type cells when suffering DNA damage caused by oxidizing or alkylating agents. Both types of cells underwent poly(ADP-ribose) polymerase 1 hyperactivation, NAD^+, and ATP depletion after severe DNA damage, only the ALKBH7-depleted cells exhibited rapid recovery of intracellular NAD^+ and ATP levels. In addition, ALKBH7-depleted cells maintained their mitochondrial membrane potential and

* This work was supported by National Basic Research Program of China 973 Programs 2011CB965304 and 2009CB825403 and National Natural Science Foundation of China Grants 31222032, 31300135, and 31370720.
[S] This article contains supplemental Movie S1.
The atomic coordinates and structure factors (codes 4QKB, 4QKD, and 4QKF) have been deposited in the Protein Data Bank (http://wwpdb.org/).
[1] To whom correspondence should be addressed. Tel.: 86-10-6273-4078; Fax: 86-10-6273-4078; E-mail: chenzhongzhou@cau.edu.cn.

homeostasis, indicating a vital role of ALKBH7 in triggering the collapse of mitochondrial membrane potential and dysfunction of mitochondria in alkylation- and oxidation-induced programmed necrosis. Besides, another study showed that the knock-out *Alkbh7* in mice led to increased body weight and body fat. Alkbh7 was found to facilitate the utilization of short-chain fatty acids (8). All of this research demonstrated the key roles of ALKBH7 in mitochondrial function.

ALKBH7 is a nonheme Fe(II)- and α-ketoglutarate (α-KG)[2]-dependent dioxygenase, one of the nine human homologs of AlkB family (termed as ALKBH1–8 plus fat mass and obesity-associated protein (FTO)) (9, 10). The Fe(II)/α-KG-dependent dioxygenases play diverse biological roles, including collagen biosynthesis, DNA repair, RNA modification, chromatin regulation/histone modification, hypoxia-sensing, and fatty acid metabolism (11). The *Escherichia coli* AlkB repairs alkylation damage with remarkably broad substrate specificity, including m^1A, m^3C, 1-methylguanine, 3-methylthymine, and etheno lesions in both DNA and RNA (12–14). Human AlkB homologs are involved in DNA repair and RNA modification with higher substrate specificity. ALKBH1 shows m^3C demethylase activity in DNA/RNA and DNA lyase activity at abasic sites (15, 16). ALKBH2 and ALKBH3 are similar to AlkB, whereas ALKBH2 prefers dsDNA and ALKBH3 is more active toward single-stranded DNA and RNA (17–20). ALKBH5 and FTO are RNA N^6-methyladenosine demethylases (21, 22). ALKBH8 catalyzes the hydroxylation of 5-methoxycarbonylmethyluridine in the anticodon stem loop of tRNA (23).

ALKBH7 does not exhibit any demethylase activity for both m^1A and m^3C lesions in single-stranded DNA/dsDNA (7, 24). Its substrate is still unknown after 10 years of assiduous research. In contrast to ALKBH7, inactivation of other AlkB family proteins leads to sensitivity rather than resistance to DNA damage (25–28). Furthermore, deletion of the *fto* gene in mice protects from obesity, whereas the *Alkbh7* knock-out mouse develops obesity (8, 29). Taken together, ALKBH7 may play a unique role distinct from the known ALKBH functions such as DNA repair or RNA modification. However, the structure and activity of ALKBH7 remain unclear.

Here, we present the atomic resolution structure of ALKBH7 in complex with Mn(II) and α-KG or *N*-oxalylglycine (NOG). Structure analyses reveal that ALKBH7 possesses the conserved active site motifs and residues of Fe(II)/α-KG-dependent dioxygenase. We demonstrate that ALKBH7 can self-hydroxylate Leu-110. Furthermore, our data reveal the differences between substrate-binding sites of ALKBH7 and other AlkB family members. Our studies not only provide an explanation why ALKBH7 has no repair activity for alkylation-damaged oligonucleotides but also indicate a potential protein hydroxylation activity of ALKBH7.

[2] The abbreviations used are: α-KG, α-ketoglutarate; DSBH, double-stranded β-helix; NRL, nucleotide recognition lid; NOG, *N*-oxalylglycine; m^1A, 1-methyladenine; m^3C, 3-methylcytosine; r.m.s.d., root-mean-square deviation; NAD^+, nicotinamide adenine dinucleotide; PDB, Protein Data Bank; HIF, hypoxia-inducible factor; Se-Met, selenomethionine.

EXPERIMENTAL PROCEDURES

Protein Expression and Purification—DNA fragments encoding various fragments of wild-type ALKBH7 and their mutants were amplified by PCR and ligated into pET-28a (Novagen) with a tobacco etch virus protease cleavage site. The final clones were verified by DNA sequencing. All proteins were expressed in *E. coli* BL21 (DE3) cells (Novagen). Cells were grown in LB at 37 °C until A_{600} reached 0.6–0.8 and then were induced for 12 h at 18 °C with 0.4 mM isopropyl β-D-1-thiogalactopyranoside. For the selenomethionine (SeMet)-labeling protein, a single colony grown at 37 °C in LB was diluted 1:1000 into M9 minimal medium containing 0.2% (w/v) glucose, 50 mg/liter of each amino acid other than methionine. Cells were grown at 37 °C until the A_{600} reached 0.3, and then 50 mg/liter SeMet (Sigma) was added. After 0.5 h of additional growth at 37 °C, cells were induced with 0.4 mM isopropyl β-D-1-thiogalactopyranoside for 16 h at 18 °C. The cultures were harvested by centrifuging at 4000 × *g* for 10 min at 4 °C and then resuspended in lysis buffer (20 mM Tris, pH 8.0, 1 M NaCl, 1 mM β-mercaptoethanol) supplemented with Triton X-100 and PMSF (Invitrogen). After sonication and centrifugation at 20,000 × *g* for 30 min at 4 °C, the supernatant was applied to His affinity beads (Bio-Rad). The column was washed with lysis buffer containing 10 mM imidazole, and the protein was eluted with lysis buffer containing 200 mM imidazole. Tobacco etch virus protease was added to the protein-containing eluent to remove the His tag at a 1:10 weight ratio overnight. The digestion production was reloaded onto His affinity beads to remove the His tag and His-tagged tobacco etch virus protease. Further purification was performed with size exclusion chromatography (Superdex™-200, GE Healthcare) using gel filtration buffer (20 mM Tris, pH 8.0, 150 mM NaCl, 2 mM dithiothreitol for native protein or 5 mM tris(2-carboxyethyl)phosphine for SeMet-labeled protein). Fractions were analyzed by SDS-PAGE, and the target protein was pooled and concentrated to 15 mg/ml for crystallization.

Crystallization and Data Collection—Mn(II) was used to replace Fe(II). To obtain ALKBH7 complex crystals, 1 mM protein was mixed with 10 mM $MnCl_2$, 10 mM α-KG, or α-KG analogs such as NOG or 2,4-pyridine dicarboxylate and then incubated on ice overnight. Initial crystallization trials were performed at 4 and 16 °C using the sitting drop vapor diffusion method. A series of truncations was tested for crystallization. The apo-ALKBH7 protein failed to crystallize, and the ALKBH7(17–215)-protein mixed with $MnCl_2$ and α-KG/NOG formed rod-shaped crystals at 4 °C in the reservoir solution of 10% PEG3K, 200 mM $MgCl_2$, 100 mM sodium cacodylate, pH 6.2. Although diffracted to 2.5 Å, these rod-shaped crystals contained a kind of crystal disorder called lattice-translocation defect (30) as revealed by the sharp and diffuse diffraction pattern (Fig. 1*A*). The smeary diffraction spots led to problems in indexing and integrating reflection intensities. The diffraction qualities of these crystals were not improved after extensive optimization of crystallization conditions or various post-crystallization treatments such as annealing and dehydration. Mutants of the ALKBH7 protein according to many strategies were applied. Finally, the Q90R mutant engineered by ALKBH7 sequence alignment between human and different species

remarkably improved the diffraction quality (Figs. 1*B* and 2). The high quality crystals were obtained by hanging drop vapor diffusion against 150 mM $MnCl_2$, 50 mM $MgCl_2$, 100 mM sodium cacodylate, pH 6.5, 10% glycerol, and 8% PEG3350 for 7 days. SeMet-labeled crystals were obtained under the same condition. For data collection, crystals were gradually transferred to a cryo-buffer (reservoir buffer supplemented with 20% ethylene glycol) and flash-frozen in liquid N_2.

The anomalous data of the selenium atom were collected on beamline BL-5A at the Photon Factory (High Energy Accelerator Research Organization). The other data were collected on beamline BL17U1 at the Shanghai Synchrotron Radiation Facility and beamline 3W1A at the Beijing Synchrotron Radiation Facility. All the data were integrated and scaled with the HKL2000 suite of programs (31). Data collection and processing statistics are shown in Table 1.

Structure Determination and Refinement—Native crystals of ALKBH7(17–215)-Q90R diffracted to 1.35 Å resolution (Table 1). Because of the low sequence homology with other structure-solved proteins (the highest sequence identity is 16%), molecular replacement was unsuccessful getting the proper phase of ALKBH7. Multiwavelength anomalous diffraction data collected from SeMet-labeled crystals were used to solve the structure.

The diffraction data of SeMet crystals were collected at the selenium peak and edge (0.97929 and 0.97943 Å) with an oscillation of 0.5° per image. However, pseudo-merohedral twinning was detected, which increased the difficulty in locating the selenium sites and structural determination. Because of low anomalous diffraction signal and twinning, no clear selenium site pattern was found using SOLVE (32). Because of only one methionine in the predicted secondary structure of this fragment, two extra methionine sites added by the R86M/L89M double mutation were found to facilitate the phasing. Initial phases were calculated by SOLVE, and phases were subsequently improved using RESOLVE (32). The figure of merit was 0.358, and the Z score was 17.1 for the solution of SOLVE. A few β-strand bundles could be automatically modeled into the electron density map by RESOLVE. Then a polypeptide model was built using COOT (33) and refined using REFAMC5 (34) in iterative cycles. Finally, the best solution was refined to an R_{work}/R_{free} values of 0.350/0.428, and the figure of merit was 0.455. Using this model, the high resolution structure was determined and built using COOT (33). After numerous rounds of model building and refinement, the structure was refined to an R_{work} of 14.7% and an R_{free} of 16.3%.

The complex structure of ALKBH7-Mn(II)-NOG was determined by molecular replacement using the ALKBH7-Mn(II)-α-KG structure as a model. The final structure was refined to an R_{work} of 15.9% and an R_{free} of 16.5%. All figures in this article displaying molecular structures were made using PyMOL (35).

LC-MS Analysis—Purified proteins (100 μM in 20 mM Tris, pH 8.0, 150 mM NaCl), 500 μM $(NH_4)_2Fe(SO_4)_2$, and 500 μM α-KG were incubated aerobically for 24 h and loaded onto SDS-PAGE. Samples were excised from Coomassie Blue-stained gels and ground to small pieces. The gel pieces were soaked in 200 μl of MilliQ-H_2O for 30 min at 37 °C and extensively washed with 100 μl of 100 mM NH_4HCO_3 three times. Then gel pieces were shrunk in 100 μl of 100 mM NH_4HCO_3 for 15 min. After removal of residual solvent and drying, the pieces were rehydrated in 10 μl of trypsin (10 ng/μl) (sequence grade, Roche Applied Science) on ice for 45 min, and then 10 μl of 25 mM NH_4HCO_3, 5% CH_3CN was added. Digestion was carried out at 37 °C overnight. The digested peptide was separated by a nano-ACQUITY UPLC BEH C_{18} 1.7 μm column (Waters), using a CH_3CN/H_2O (0.1% formic acid) gradient. MS utilized a Q Exactive Hybrid Quadrupole-Orbitrap mass spectrometer (Thermo Scientific) that was set to detect positive ions over the 300–1800 m/z range.

Microscale Thermophoresis—The binding affinity of α-KG toward ALKBH7 was measured using microscale thermophoresis with Monolith NT.115 (NanoTemper Technologies GmbH, München, Germany). ALKBH7 was labeled with a fluorescent dye NT-647 (cysteine-reactive) according to the manufacturer's manual. For the assay, 10 μl of 10 μM labeled protein in a buffer containing 20 mM Tris, pH 8.0, 150 mM NaCl, 0.005% Tween 20 was mixed with 10 μl of α-KG at various concentrations. The final concentrations were from 0.75 to 6250 μM for α-KG. After incubation for 30 min at room temperature, 10 μl of the mixture were loaded into standard treated capillaries. Thermophoresis was measured at 25 °C for 30 s with 20% LED power and 40% infrared laser power. Data of three independent measurements were combined and analyzed using the NTAnalysis software (NanoTemper Technologies GmbH).

RESULTS

Structure Determination of ALKBH7—Predicted as a mitochondrial targeting sequence (7), the N-terminal 17 residues of ALKBH7 were deleted to promote prokaryotic expression. After extensive screening, truncation of the C-terminal 6 residues was found to facilitate protein crystallization. The apoprotein failed to crystallize, whereas the ALKBH7·Mn(II)·α-KG/NOG complex did, indicating a more ordered conformation after binding ligands. However, the wild-type protein crystal produced a poor diffraction pattern (Fig. 1*A*). After further screening, a Q90R mutant selected according to the protein sequence of *Bos taurus* (Fig. 2) was found to greatly improve the diffraction quality (Fig. 1*B*). However, the structure was not solved because no similar structures were available, and the anomalous diffraction signal of SeMet-labeled protein crystals was low. The R86M/L89M double mutation introducing two additional methionine residues was found to facilitate structural determination. The structure of ALKBH7 in complex with Mn(II) and α-KG was solved using the multiwavelength anomalous diffraction signal of SeMet-labeled protein crystals and was refined to 1.35 Å resolution for native protein crystals. There are three protein molecules in the asymmetric unit. We rebuilt Mn(II), α-KG, and 189 residues for each ALKBH7 molecule, although no electron density was observed for residues 100 and 207–215. The structure of ALKBH7 in complex with Mn(II) and NOG was solved using molecular replacement and refined to 2.0 Å resolution. Interestingly, only two NOG molecules were found in the trimeric structure. An overlay of ALKBH7-Mn(II)-α-KG and ALKBH7-Mn(II)-NOG structures revealed little difference in the overall conformation with a root mean square deviation (r.m.s.d.) of 0.4 Å. In addition, the

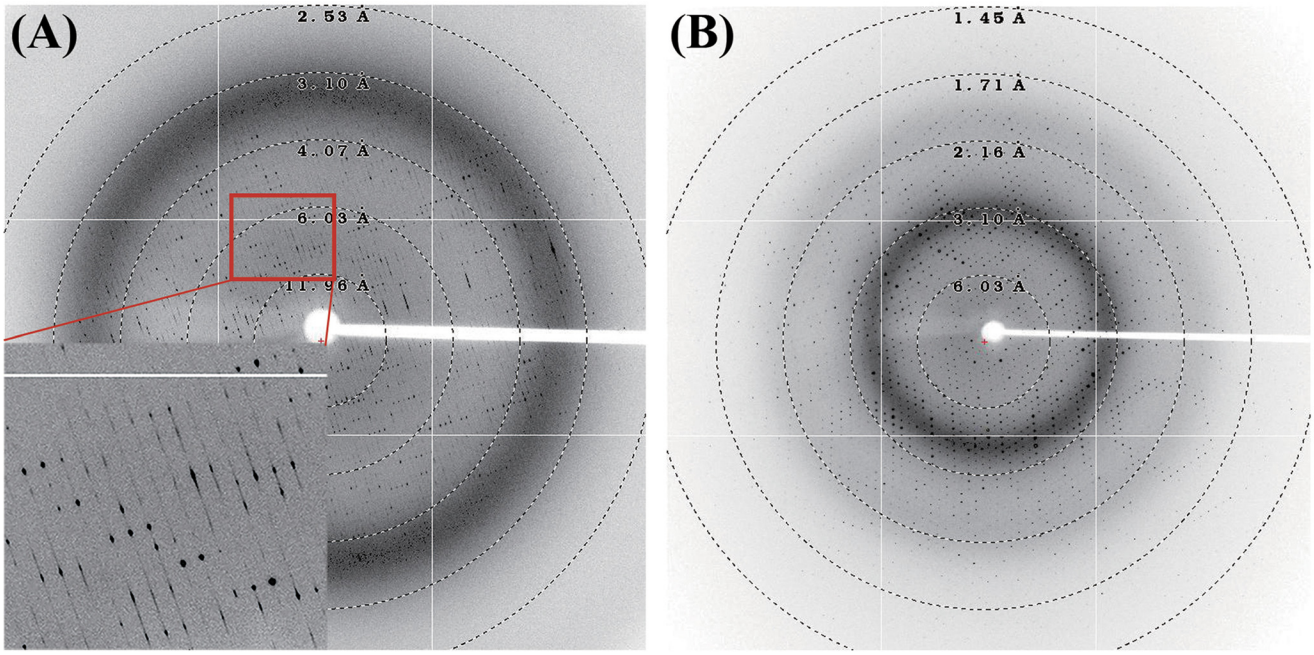

FIGURE 1. **X-ray diffraction patterns of ALKBH7 and Q90R mutants.** *A,* wild-type ALKBH7 Mn(II)·α-KG complex crystals display a sharp and diffuse diffraction pattern with a lattice-translocation defect. The enlargement is in the *left lower panel*. *B,* Q90R mutant of ALKBH7 significantly improves the *X*-diffraction quality.

R86M/L89M double mutation (Table 1) also did not alter the overall structure with an r.m.s.d. of 0.3 Å.

Overall Structure of ALKBH7·Mn(II)·α-KG/NOG Complexes Show a Conserved DSBH Fold—A total of 10 β-strands surrounded by four α-helices make up the central structure of ALKBH7 (Fig. 3 and supplemental Movie S1). As expected, the catalytic core of ALKBH7 contains a DSBH fold conserved in the Fe(II)/α-KG-dependent dioxygenase superfamily (36). However, only seven β-strands of the DSBH are observed in ALKBH7. Four β-strands (β4, β5, β8, and β10, also referring to βI, βIII, βVI, and βVIII of DSBH) form the major β-sheet, and three β-strands (β6, β7, and β9, also referring to βIV, βV, and βVII of DSBH) plus a loop between β4 and β5 form the minor β-sheet. Strands β1, β2, and helix α1 lie in the N terminus of the DSBH fold, which is further buttressed by helices α2 and α3. Strand β3 between helices α2 and α3 is anti-parallel to strand β4 and extends the major β-sheet of the DSBH.

Inserts frequently occurring in the loop between βIV and βV of DSBH are discovered to be involved in binding substrates in the Fe(II)/α-KG-dependent dioxygenases (36, 37). Such inserts are found in AlkB, ALKBH2, ALKBH3, and ALKBH5 (Fig. 2) (19, 20, 38). Unlike them, the loop between βIV (β6) and βV (β7) of ALKBH7 is short and contains only 6 residues (Figs. 2 and 3), similar to that of HIF prolyl-hydroxylase PHD2 (39). Beyond that, the long loop (residues 180–195) between βVII (β9) and βVIII (β10) (Figs. 2 and 3 and supplemental Movie S1), which forms the outer wall of the minor β-sheet in ALKBH7, is rarely found in the Fe(II)/α-KG dioxygenase superfamily.

Although wild type and Q90R mutant were monomeric in solution, they crystallized as a homotrimer in the space group $P2_1$ (Fig. 4*A*). The Q90R mutation introduces a stabilization network between Arg-90 of one ALKBH7 molecule and Glu-44 and Arg-91 of the adjacent ALKBH7 molecule (Fig. 4*B*), which might facilitate the crystal packing. This mutation locates on the helix α3 and is far away from the active site. Except in the active center, Mn(II) ions are also found at the molecule-molecule interface. Interaction between residues His-65 of one ALKBH7 molecule and Glu-62 and Glu-75 of the neighboring ALKBH7 molecule via a Mn(II) ion promotes the formation of the crystallographic trimer (Fig. 4*C*). Another significant lattice contact involves a Mn(II) ion surrounded by three Glu-189 residues from three ALKBH7 molecules (Fig. 4*D*).

ALKBH7 Has a Unique Active Center—The HX(D/E) . . . X_n . . . H facial triad motif of ALKBH7 coordinates the metal ion at the active site, which is conserved in the Fe(II)/α-KG-dependent dioxygenase superfamily (36). The differential electron density map clearly shows that the Mn(II) is coordinated in an octahedral manner by two oxygen atoms of α-KG, one water molecule and the side chains of His-121, Asp-123, and His-177 (Fig. 5*A*). The observed distances for residues coordinating with the metal ion correspond to normal values as other ALKBH family members. The cofactor α-KG chelates Mn(II) in a bidentate manner via its c-1 carboxylate *trans* to His-177 and c-2 keto group *trans* to Asp-123. α-KG is further stabilized by electrostatic interaction with Arg-197 and Arg-203 at the both ends of β10 (βVIII), which is conserved in AlkB family (Figs. 2 and 5*A*).

In most of the AlkB family proteins, the α-KG c-5 carboxylate hydrogen bonds to the side chain of tyrosine from DSBH βI (Fig. 5, *D–H*). However, the α-KG-binding tyrosine comes from DSBH βVI in ALKBH7 and FTO (Fig. 5, *A* and *I*). Moreover, this α-KG c-5 carboxylate-binding tyrosine (Tyr-165) is highly conserved among ALKBH7 from different species (Fig. 2). The α-KG c-5 carboxylate also forms another hydrogen bond with the side chain of asparagine from βVIII in AlkB, ALKBH2, or ALKBH3 (Fig. 5, *D–F*) and with that of Ser-199 from βVIII (β10) in ALKBH7 (Fig. 5*A*). Furthermore, the α-KG c-1 carboxylate oxygen usually forms a hydrogen bond with asparagine

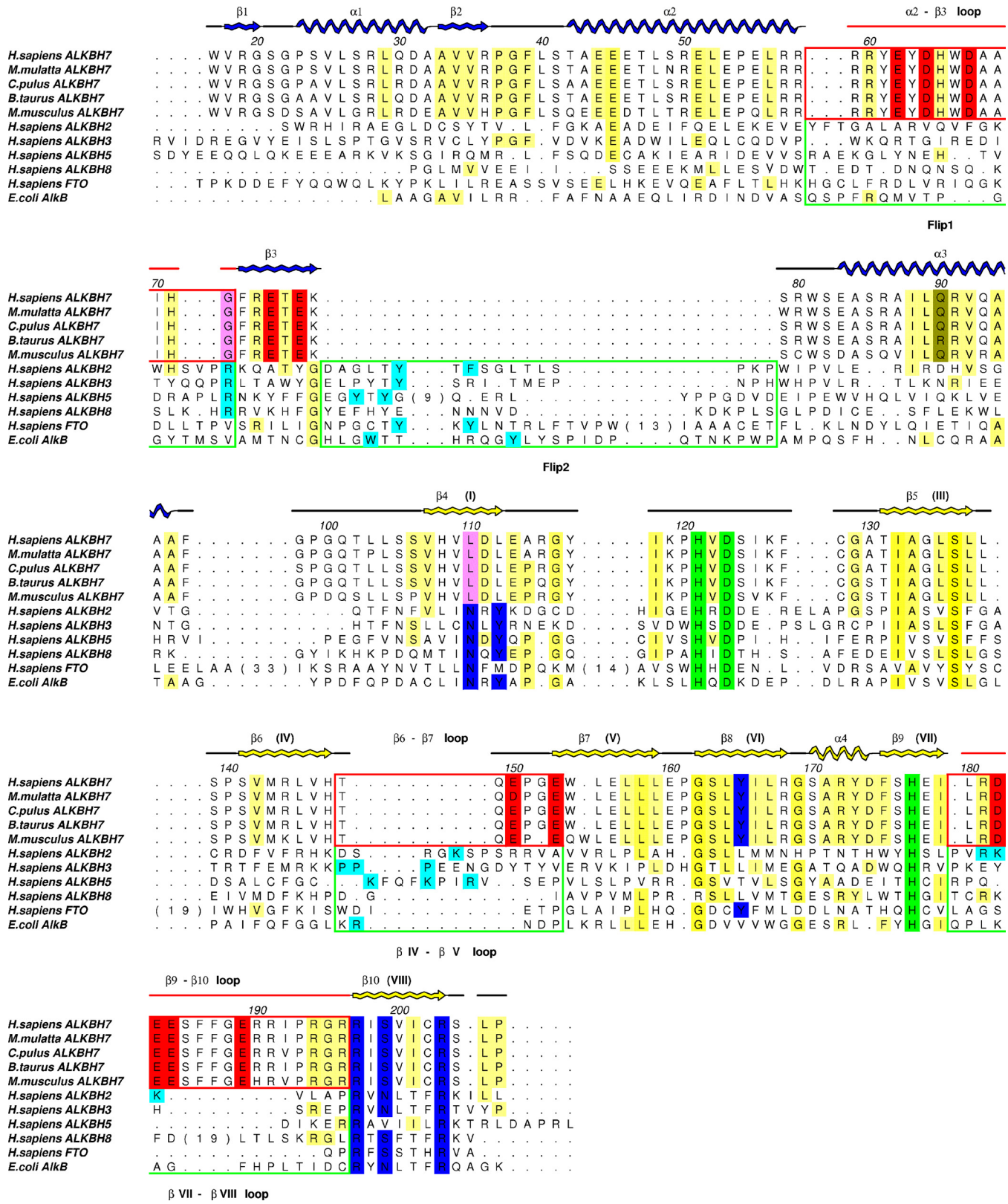

FIGURE 2. **Structure-based sequence alignment of ALKBH7 homologs from different species and other AlkB family members.** Listed below are the ALKBH7 homolog names followed by GenBank™ accession number and (% identity) to the human ALKBH7: *Homo sapiens* gi|14150066| (100%); *Macaca mulatta* gi|109123098 (97.3%); *Canis pulus* gi|73987027 (93.7%); *Bos taurus* gi|114051906 (92.8%); and *Mus musculus* gi|21313470 (81.9%). Structures used are as follows: ALKBH2 (PDB code 3BUC); ALKBH3 (PDB code 2IUW); ALKBH5 (PDB code 4NRO); ALKBH8 (PDB code 3THT); FTO (PDB code 3LFM); and AlkB (PDB code 3BIE). Secondary structural elements are represented according to the structure of ALKBH7. Residue numbers are labeled according to the sequence of ALKBH7. Residues ligating the catalytic metal ion are colored *green,* and residues binding α-KG are colored *blue*. Residues marked with *green box* indicate those forming Flip1, Flip2, βIV-βV loop, and βVII-βVIII loop of ALKBH2, ALKBH3, ALKBH5, ALKBH8, FTO, and AlkB, the nucleobase or phosphate backbone-binding residues are colored *cyan*. Residues marked with *red box* indicate those forming α2-β3 loop, βIV-βV loop, and βVII-βVIII loop of ALKBH7, and the conserved negative residues are colored *red*.

TABLE 1
Data collection and refinement statistics of ALKBH7 complexes
Three crystal experiments are shown for each structure.

	Selenium peak	Selenium edge	SeMet-ALKBH7-Mn^{2+}-α-KG (R86M/L89M/Q90R)	ALKBH7-Mn^{2+}-α-KG (Q90R)	ALKBH7-Mn^{2+}-NOG (Q90R)
Data collection					
Wavelength	0.97929	0.97943	0.97929	1.0000	1.0000
Space group	$P2_1$	$P2_1$	$P2_1$	$P2_1$	$P2_1$
Cell dimensions					
a, *b*, *c* (Å)	66.7, 82.8, 66.7	66.7, 82.8, 66.7	66.7, 82.8, 66.7	66.4, 82.0, 66.4	66.4, 82.0, 66.1
α, β, γ (°)	90.0, 119.9, 90.0	90.0, 119.9, 90.0	90.0, 119.9, 90.0	90.0, 120.0, 90.0	90.0, 119.9, 90.0
Resolution (Å)[a]	50.0-2.30 (2.34-2.30)	50.0-2.30 (2.34-2.30)	50.0-2.60 (2.64-2.60)	50.0-1.35 (1.37-1.35)	50.0-2.0 (2.03-2.0)
*R*merge (%)	8.6 (27.7)	9.0 (38.9)	7.7 (22.2)	9.6 (31.6)	7.0 (36.4)
I/σ	39.4 (3.6)	37.0 (3.3)	46.6 (9.2)	44.1 (4.5)	35.9 (6.4)
Completeness (%)	71.8 (16.1)	74.2 (23.4)	90.5 (51.0)	91.9 (61.0)	96.7 (80.5)
Total no. of reflections	267923	282134	249,456	620,491	149,842
Unique reflections	20147	20757	17,632	124,116	40,730
Redundancy	13.3 (4.7)	13.6 (6.3)	14.1 (10.0)	5.0 (3.2)	3.7 (3.5)
Refinement					
Resolution (Å)			50.0-2.60 (2.64-2.60)	50.0-1.35 (1.37-1.35)	50.0-2.0 (2.03-2.0)
No. of reflections			16,706 (667)	117,785 (5898)	38,211 (2057)
R_{work}/R_{free} (%)			15.9/18.1	14.7/16.3	15.9/16.5
No. of atoms					
Protein			4476	4502	4506
Ligand/ion			37	37	24
Water			54	731	159
B-factors(Å^2)					
Protein			28.4	17.6	35.5
Ligand/ion			24.3	13.2	30.2
Water			21.9	29.3	35.5
r.m.s.d.					
Bond lengths (Å)			0.007	0.008	0.009
Bond angles (°)			1.152	1.348	1.324
Ramachandran plot (%)[b]			93.4/6.0/0/0.6	94.5/4.9/0/0.6	90.5/8.9/0/0.6

[a] Statistics are for highest resolution shell.
[b] Residues in most favored, additional allowed, generously allowed, and disallowed regions of the Ramachandran plot are shown.

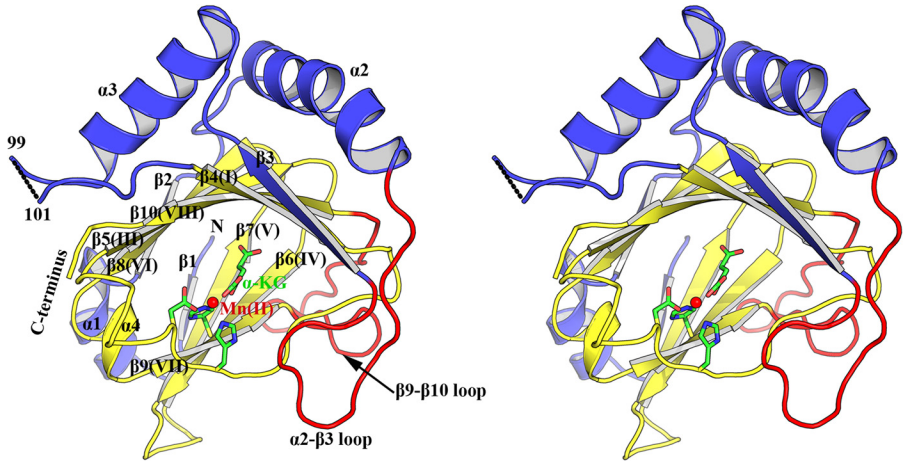

FIGURE 3. **Overall structure of ALKBH7 in complex with Mn(II) and α-KG.** Stereoview of the ALKBH7(17–206) structure in the presence of α-KG and Mn(II). The Mn(II) ion is shown as a *red sphere*. Key residues as well as α-KG are shown as *green sticks*. Secondary structures are labeled. The α2-β3 loop and β9-β10 loop are highlighted in *red*.

from βI in AlkB family. But no such hydrogen bond was observed in ALKBH7, a unique feature of it (Fig. 5, *A* and *D–I*). A highly conserved Leu-110 among ALKBH7 from different species lies in the equivalent position of the above asparagine (Fig. 2).

The absence of a hydrogen bond between α-KG c-1 carboxylate and ALKBH7 would lead to weaker binding affinity than those previously reported α-KG-dependent oxygenases. Consistently, the dissociation constant (K_d) was determined to be 80.9 ± 8.12 μM using microscale thermophoresis (Fig. 5*C*). The weak binding of cofactor is further proven by the rotation of the c-1 carboxylate of NOG in the crystal structure (Fig. 5*B*). The distance between c-1 carboxylate and metal ion increases from 2.0 to 2.8 Å in the ALKBH7·Mn(II)·NOG complex structure compared with that in the ALKBH7·Mn(II)·α-KG complex structure.

Besides the α-KG binding residues, other residues in the α-KG binding cavity of ALKBH7 are mainly hydrophobic. These residues are derived from β-strands β4 (Leu-110 and Leu-112), β5 (Ile-132), β6 (Met-143 and Leu-145), β7 (Leu-155, Leu-157, and Leu-159), β8 (Tyr-165 and Leu-167), β9 (Ile-179), and β10 (Ile-201).

Another interesting discovery is the post-translational modification of Leu-110 (Fig. 5*A*). A similar but not the same post-

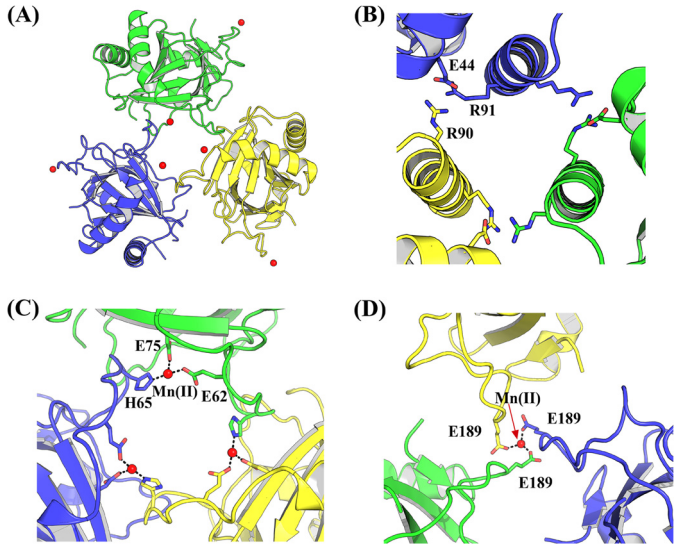

FIGURE 4. **Crystallographic trimer of ALKBH7.** *A,* schematic representation of the crystallographic trimer of ALKBH7. The three molecules are shown in *green, blue,* and *yellow*. Mn(II) ions at the molecule-molecule interface are shown as *red spheres*. *B,* stabilization of Arg-90 by electrostatic interactions and hydrogen bonds with Glu-44 and Arg-91 of the adjacent ALKBH7. *C,* detailed interaction between neighboring ALKBH7 molecules in the asymmetric unit. Mn(II) is bound by His-65 of one ALKBH7 and Glu-62, Glu-75 of the adjacent ALKBH7. *D,* detailed interaction between neighboring ALKBH7 molecules in the symmetric unit. Mn(II) ion is chelated by Glu-189 from three molecules.

translational modification was reported in ALKBH3 (19). Differences will be discussed in detail below.

Comparison with Other AlkB Family Members Reveals Several Unique Features of ALKBH7—Despite the vital role in alkylation- and oxidation-induced programmed necrosis and metabolism of short-chain fatty acids, the main substrate of ALKBH7 remains unknown. Comparison of ALKBH7 and other AlkB family members may shed light on the open question. Although ALKBH1 was reported as a histone H2A demethylase (40) and ALKBH4 was shown to mediate demethylation of a monomethylated site (K84me1) in actin *in vivo* (41), all structure-solved AlkB family members are nucleic acid oxygenases whose substrates are either DNA or RNA. Here, structural comparison of ALKBH7 and other AlkB homologs demonstrates several unique features that make ALKBH7 significantly different from the nucleic acid oxygenases.

Superimposed to the solved AlkB family structures, the most significant structural difference of ALKBH7 rests on the motif referring to as the "nucleotide recognition lid (NRL)." All structurally characterized nucleic acid oxygenases possess a conserved NRL that constitutes the nucleobase-binding cavity (Fig. 6*A*). NRL is further divided into two parts named "Flip1" and "Flip2." Although Flip1 determines double-strand *versus* single-strand substrate recognition of ALKBH2 and ALKBH3 (18), Flip2 provides residues interacting with the modified nucleobase. In AlkB, ALKBH2, FTO, or ALKBH5, Trp-69, Phe-124, Tyr-108, or Tyr-141 (Fig. 5, *D, E, I,* and *G*) in Flip2 binds the modified nucleobase through aromatic stacking interaction (20, 38, 42–44). Y108A mutant in FTO and Y141A mutant in ALKBH5 abolished their activity (43, 44). Furthermore, Tyr-76 of AlkB and Tyr-122 of ALKBH2 in Flip2 interact with the N6 atom of the m^1A substrate (Fig. 5, *D* and *E*) (20). Tyr-143 of ALKBH3, Tyr-139 of ALKBH5, and Tyr-106 of FTO are in the equivalent position (Fig. 5, *F, G,* and *I*). However, structural comparison and sequence alignment of AlkB family members clearly reveal the absence of Flip2 in ALKBH7 (Figs. 2 and 6*A*). The lack of Flip2 in ALKBH7 leads to a solvent-exposed active site and a loss of nucleobase binding ability.

Moreover, the conformation of α2-β3 loop in ALKBH7 is different from that of Flip1 in other AlkB family members and the residues in Flip1, which are important in binding nucleobase or phosphate backbone, are also absent in the α2-β3 loop (Fig. 6*B*). Arg-110 was found to interact with the substrate phosphate backbone in ALKBH2·dsDNA complex (20). Arg-131 of ALKBH3 in the equivalent site is positioned to make contact with the N3 atom of m^1A, and R131A mutant was shown to be inactive (19). However, Gly-72 is located in the equivalent position of ALKBH7 (Figs. 2 and 6*B*). The absence of a nucleic acid-binding residue may greatly affect the binding to nucleic acid. Furthermore, structural superimposition of ALKBH7 and the AlkB·dsDNA or ALKBH2·dsDNA complex demonstrates that the α2-β3 loop of ALKBH7 would crash with the modified DNA strand (Fig. 6*C*). The α2-β3 loop does not seem to have enough flexibility to undergo conformational change due to the rather low temperature factor in the solved structures.

Previous studies have demonstrated that a positively charged groove and the βIV-βV loop are needed to bind nucleic acids (19, 20, 38, 42, 44, 45). The minor β-sheet plus βIV-βV loop of DSBH create the nucleic acid binding groove in nucleic acid oxygenases (Fig. 6, *D* and *E*). Arg-161 located at the apex of the βIV-βV loop of AlkB is important in the recognition of the damaged nucleobases. ALKBH2 has a long βIV-βV loop carrying nucleic acid-binding residues Arg-198 and Lys-205 and a short βVII-βVIII loop with a positively charged RKK sequence (Arg-241–Lys-243). The βIV-βV loop is not visible in the crystal structure of ALKBH3, but three consecutive prolines in this loop form a proline-rich pinch that has been shown to play a role in DNA damage scanning. In ALKBH5, the βIV-βV loop includes basic residues (Lys-231, Lys-235, and Arg-238), which form a positively charged groove. However, the counterpart (β6-β7 loop) of ALKBH7 only contains 6 residues (Figs. 2 and 3), and this short loop is negatively charged with two acidic residues (Glu-150 and Glu-153). In addition to this, the electrostatic potential map of ALKBH7 demonstrates a continuous negatively charged surface compared with the positively charged groove of nucleic acid oxygenases (Fig. 6*E*).

Structural comparison of the DSBH domain of AlkB family members reveals an additional long loop between βVII and βVIII (β9 and β10) in ALKBH7, which forms the outer wall of the minor β-sheet (Fig. 6*D*). Several conserved acidic residues (Asp-182, Glu-183, Glu-184, and Glu-189) in the βVII-βVIII (β9-β10) loop lead to the negatively charged surface of ALKBH7 (Figs. 2 and 6*E*). It is worth mentioning that ALKBH8 has a long βVII-βVIII loop as well (46). Because the binding of tRNA is through its RNA recognition motif domain, this loop of ALKBH8 is proposed to mediate regulatory interactions remotely from the active site. There are also several acidic residues (Glu-306, Asp-316, and Asp-319) in the loop of ALKBH8. The similarity of the βVII-βVIII loop between ALKBH7 and

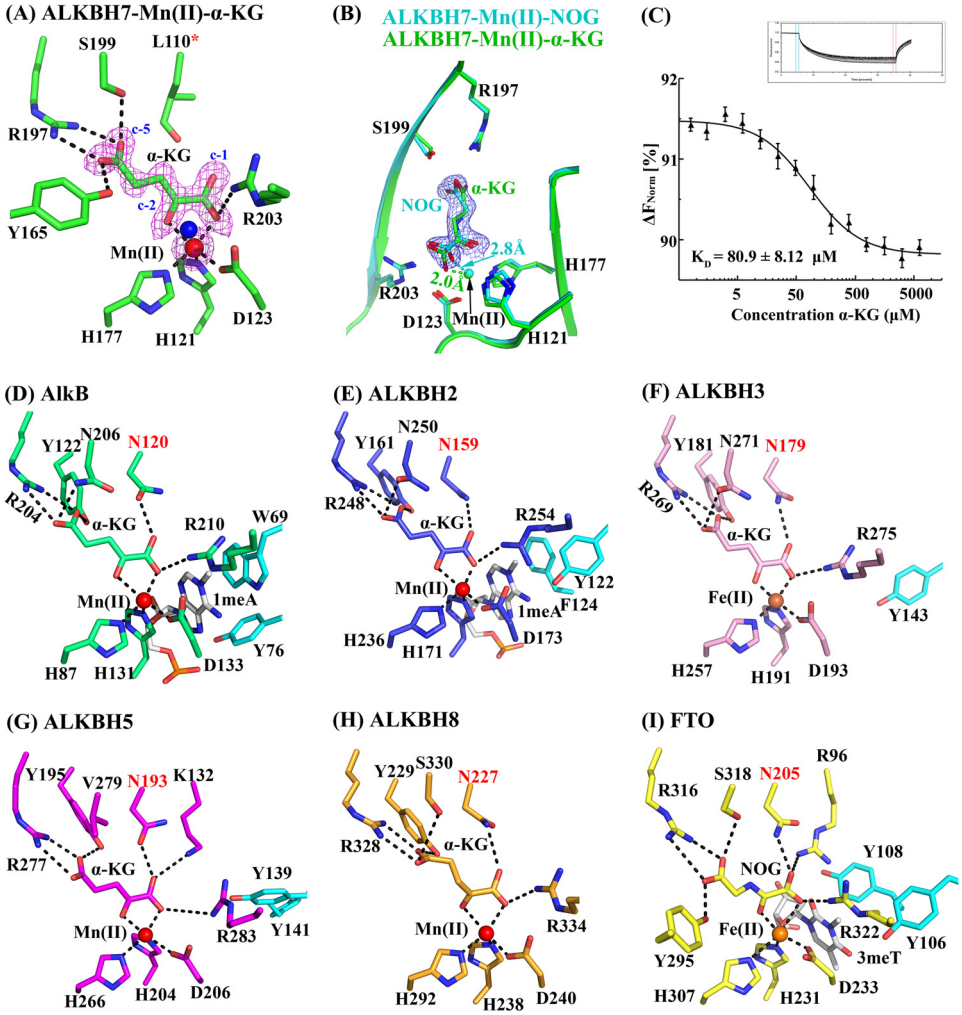

FIGURE 5. **ALKBH7 has an unusual active center.** *A,* view of the ALKBH7 active site residues, α-KG and Mn(II). $F_o - F_c$ (3.0σ, *magenta mesh*) is calculated after omitting α-KG and Mn(II). The α-KG and its interacting residues are shown as *green sticks*. The Mn(II) ion is shown as a *red sphere* and water is shown as a *blue sphere*. *B,* conformation comparison of α-KG and NOG in the two structures. ALKBH7-NOG complex is colored *cyan,* and ALKBH7-α-KG complex is colored *green*. $F_o - F_c$ electron density map (*blue mesh*) of NOG is contoured at 2.0σ. *C,* equilibrium binding analysis of ALKBH7 with α-KG in the presence of the Mn(II) ion using microscale thermophoresis (*MST*). *D–I,* active center of other AlkB family members. AlkB (*lime green*, PDB code 3BIE), ALKBH2 (*blue*, PDB code 3BUC), ALKBH3 (*pink*, PDB code 2IUW), ALKBH5 (*magenta*, PDB code 4NRO), ALKBH8 (*orange*, PDB code 3THT), FTO (*yellow,* PDB code 3LFM), respectively. Residues of the nucleotide recognition lid (*NRL*) Flip2, which are important in binding nucleobase (*white sticks*), are colored *cyan*. Note that Flip2 of ALKBH8 is completely disordered so the residues are not shown. The asparagine that forms a hydrogen bond with α-KG c-1 carboxylate oxygen is highlighted in *red*. The Mn(II) ion is shown as a *red sphere* and Fe(II) ion is shown in *brown sphere*.

ALKBH8 indicates this loop may also serve as a binding site for substrates or partner proteins in ALKBH7.

Similar Conformation of ALKBH7 and Fe(II)/α-KG-dependent Dioxygenase PHD2—Significant differences between ALKBH7 and other AlkB family members in both structure and assay suggest a distinct function of ALKBH7 from other known ALKBH members. Therefore, a structural similarity search with the DALI server (47) was carried out to investigate the potential function of ALKBH7 by structural comparison.

Besides AlkB family members, the best match is the human PHD2, the HIF prolyl 4-hydroxylase (PDB code 3HQR; r.m.s.d. 2.7 Å for 155 Cα atoms, Z-score = 14.3 and sequence identity 10%) (48). PHD2 is a cellular oxygen sensor which catalyzes the post-translational formation of 4-hydroxyproline in HIF-1α proteins (49, 50). Structural alignment of ALKBH7 and PHD2 exhibits a similar conformation except for the longer substrate binding lid of PHD2 in the equivalent position of α2-β3 loop of ALKBH7 and an extra α-helix in the C terminus of PHD2 (Fig. 7*A*). Interestingly, no major steric hindrance is found between the FIH1-α CODD peptide and ALKBH7 (Fig. 7*B*). Although residues forming the α-KG binding pocket are not strictly conserved between PHD2 and ALKBH7, the active site cavity of PHD2 is also predominantly lined by hydrophobic residues as ALKBH7.

Binding of HIF-1α COOD peptide to PHD2 is mainly through hydrophobic interactions (48). In ALKBH7, three acidic residues (Glu-62, Asp-64, and Asp-67) in the α2-β3 loop along with two acidic residues (Glu-75 and Glu-77) in strand β3 create a negatively charged cleft opening into the active site (Figs. 2 and 6*E*). Furthermore, there are two acidic residues (Glu-207 and Glu-213) in the disordered C terminus, which may be involved in binding substrates. These features indicate that ALKBH7 could interact with a substrate containing positive charges, which is different from the FIH1-α CODD peptide. Combined with the structural similarity between ALKBH7 and PHD2, proline and lysine/arginine-containing peptides,

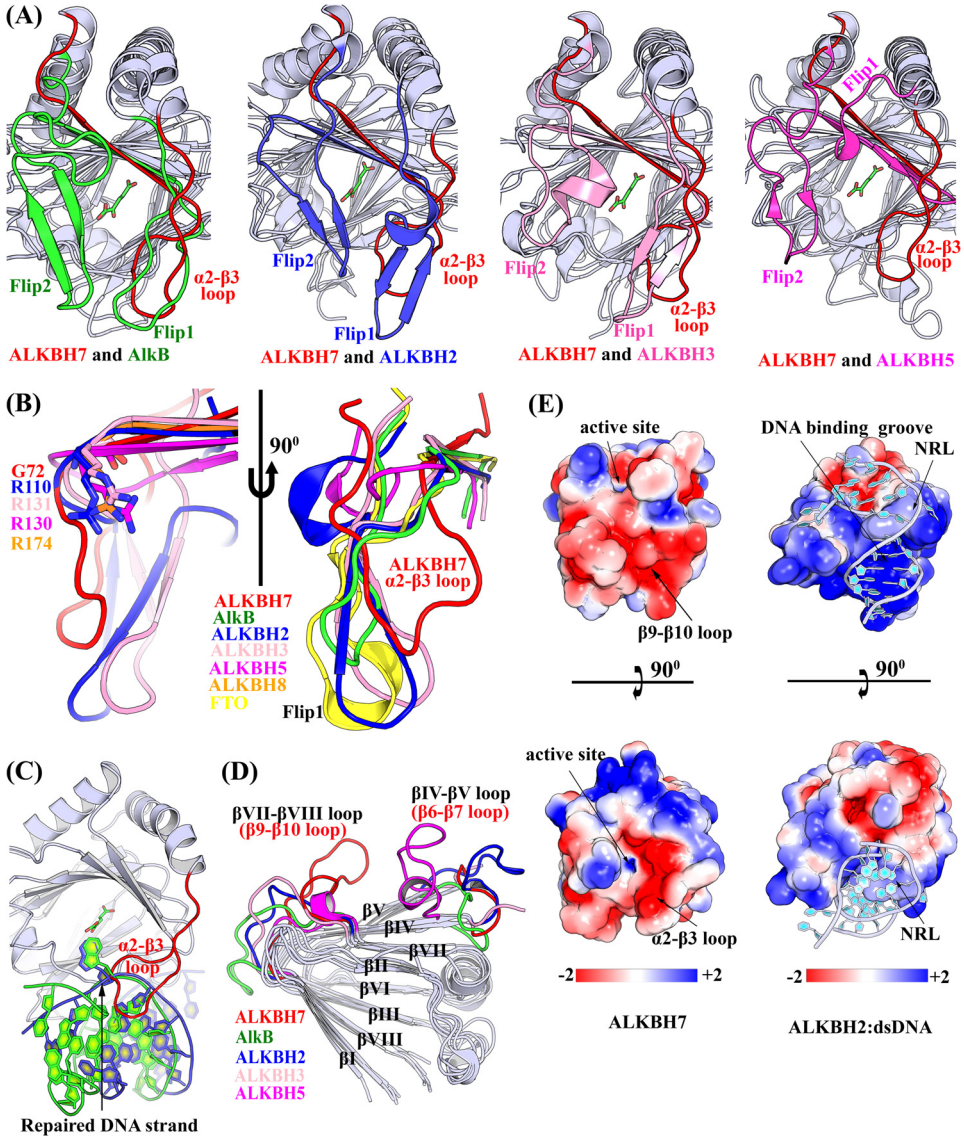

FIGURE 6. **ALKBH7 lacks the nucleotide recognition lid, which is essential for binding nucleobase and exhibits a solvent-exposed active site.** *A,* structural superimposition of ALKBH7 and other AlkB family members. The conserved nucleotide recognition lids of AlkB (*green*), ALKBH2 (*blue*), ALKBH3 (*pink*), and ALKBH5 (*magenta*) are *highlighted*. The Flip1 and Flip2 of the nucleotide recognition lid are labeled, and the corresponding motifs of ALKBH7 are colored *red*. Structure comparison clearly reveals the absence of Flip2 in ALKBH7. *B,* comparison of Flip1 of the nucleic acid oxygenases and the α2-β3 loop of ALKBH7. The conformation of α2-β3 loop is different from that of Flip1 and the α2-β3 loop lacks arginine residues that are important in binding nucleobase and phosphate backbone. *C,* superimposition of ALKBH7, AlkB-dsDNA (*green*), and ALKBH2-dsDNA (*blue*) complexes. The α2-β3 loop of ALKBH7 (*red*) overlaps with the repaired DNA strands. Note: AlkB and ALKBH2 are not shown. *D,* comparison of the DSBH fold of AlkB family members. The βIV-βV loop and βVII-βVIII loop are highlighted. *E,* electrostatic surface representation (basic in *blue*; acidic in *red*) of ALKBH7 and ALKBH2. The surface of ALKBH7 in equivalent position with the nucleic acid binding groove of other AlkB family members is negatively charged. The active site of ALKBH7 is solvent-exposed, and the cleft opening into the active site is negatively charged.

which could be the substrates of ALKBH7, need to be further identified.

Leu-110 Is Hydroxylated in the ALKBH7·α-KG Complex—An extra electron density of Leu-110 was found in the ALKBH7·α-KG complex (Fig. 8), indicating a post-translational modification for Leu-110. LC-MS was further used to identify this modification. The tryptic digest of ALKBH7 was separated by nanoACQUITY UPLC and detected via MS analysis. A mass shift of +16 Da was found in MS analyses of the co-eluted modified and unmodified peptides (Fig. 9*A*). This result demonstrated Leu-110 was partially hydroxylated. MS analysis of the L110A mutant only showed the unmodified peptide, further confirming that Leu-110 is the hydroxylated residue (Fig. 9*B*). Self-hydroxylation of Leu-110 was furthermore supported by loss of self-hydroxylation in the H121A/D123A and R197A/R203A mutants (Fig. 9, *C* and *D*). These two mutants disturb the metal ion or α-KG binding and thus lack catalytic activity. Observation of self-hydroxylation suggests that ALKBH7 could catalyze post-translational modification of its substrate. Moreover, the Q90R mutation did not alter the self-hydroxylation.

The modification of ALKBH7 Leu-110 may have resulted from an attack by a hydroxyl radical formed by the uncoupled reaction. It is commonly thought that this uncoupled reaction could arise from binding inhibitors or poor substrates and could also occur in the absence of a primary substrate. There is evidence that autocatalyzed oxidative modifications happen to

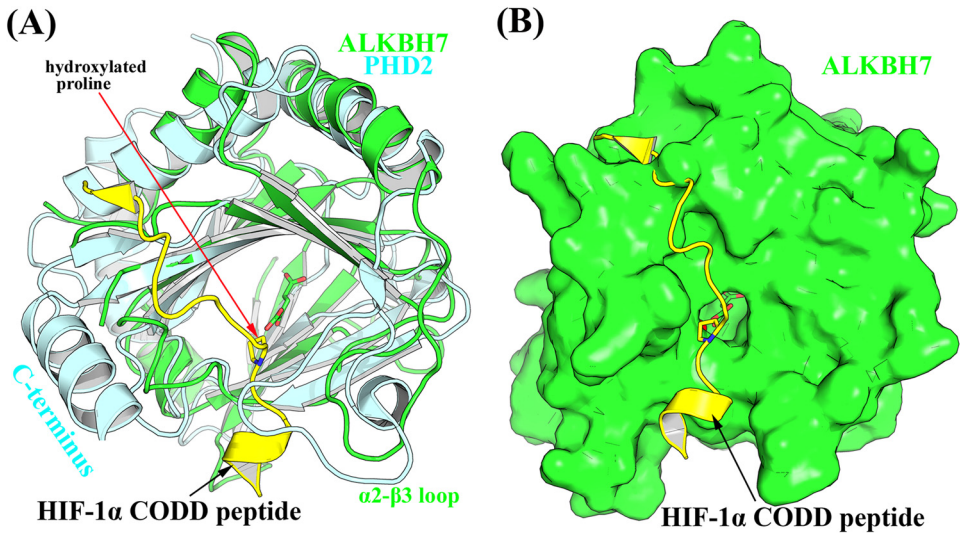

FIGURE 7. **Structural comparison of ALKBH7 and PHD2.** *A*, structural superimposition of ALKBH7 and PHD2 in complex with HIF-1α CODD peptide (PDB code 3HQR). ALKBH7, PHD2, and HIF-1α CODD peptides are colored *green*, *pale cyan*, and *yellow*, respectively. The hydroxylated proline and α-KG are shown as *sticks*. C terminus of PHD2 and α2-β3 loop of ALKBH7 are labeled. *B*, surface representation of ALKBH7 (*green*) and the HIF-1α CODD peptide (*yellow*).

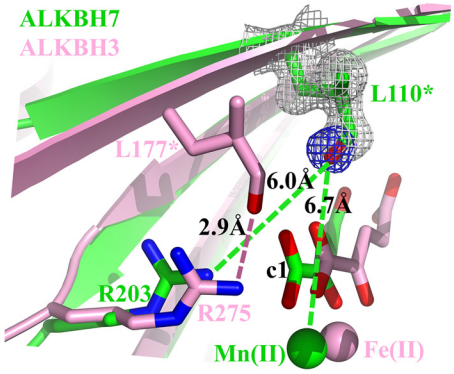

FIGURE 8. **Structure of the hydroxylated leucine in both ALKBH3 and ALKBH7.** ALKBH3 and ALKBH7 are colored *pink* and *green*, respectively. The α-KG and α-KG c-1 carboxylate coordinating arginine and hydroxylated leucine are shown as *sticks*. The metal ions are shown as *spheres*. $2F_o - F_c$ (contoured at 1σ, in *gray*) and $F_o - F_c$ (contoured at 3σ, in *blue*) were calculated after omitting the Leu-110 modification (assigned Oϵ).

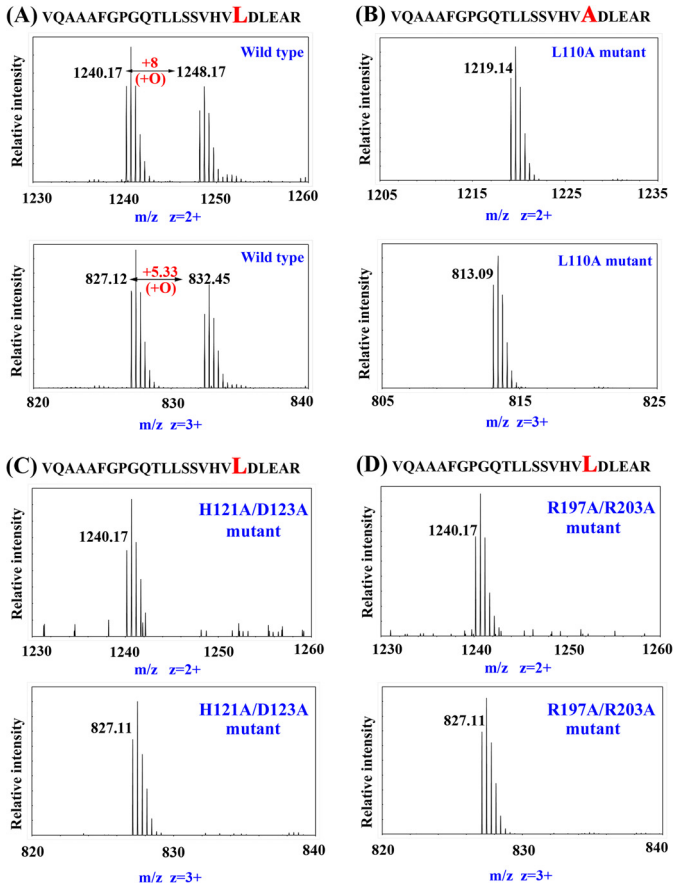

FIGURE 9. **MS spectra reveals self-hydroxylation of Leu-110 in ALKBH7.** *A*, MS analysis of the tryptic digest of ALKBH7 showed that the tryptic fragment containing Leu-110 (92–115, 2478.32 Da) appeared as m/z = 1240.17 (unmodified) and 1248.17 (+8) as z = 2+ ions; m/z = 827.12 (unmodified) and 832.45 (+5.33) as z = 3+ ions, demonstrating a +16-Da modification. MS analysis of the tryptic digest of ALKBH7 L110A (*B*), H121A/H123A (*C*), and R197A/R203A (*D*) mutants showed that the fragment 92–115 only appeared at the unmodified mass. Note that the mass of the fragment 92–115 in L110A mutant is 2436.28 Da.

Fe(II)/α-KG-dependent dioxygenases (51). Hydroxylation of Leu-177 was also found in ALKBH3 (19). Leu-177 locates in the central position of the active center of ALKBH3 serving as a "buffer stop" to prevent penetration of alkylated purines too deep in the catalytic pocket. The leucine is conserved in AlkB, ALKBH2, and FTO. It is proposed that formation of the hydrogen bond between the oxidized Leu-177 and Arg-275 negatively affects the coordination of α-KG and inactivates ALKBH3 to avoid generation of reactive oxygen species. L177E and L177Q mutants mimicking the oxidized leucine abolished the catalytic activity of ALKBH3. Fu *et al.* (7) generated the L110Q mutant of ALKBH7 to inactivate the protein according to the L177Q mutant of ALKBH3. However, the mutant could promote necrosis as well as the wild type. Structural superimposition of ALKBH3 and ALKBH7 exhibits a different location of ALKBH3 Leu-177 and ALKBH7 Leu-110 (Fig. 8). Actually, the corresponding residue of ALKBH3 Leu-177 is His-108 in ALKBH7 and not Leu-110. The hydroxylated Leu-110 is 6.0 Å away from the α-KG-binding Arg-203 of ALKBH7, so there is no interaction between them. Moreover, the hydroxyl group of the hydroxylated Leu-110 is 6.7 Å away from the catalytic iron center. Because the hydroxylated Leu-110 cannot negatively affect α-KG and the catalytic iron ion in ALKBH7, it is not surprising

that L110Q mutant of ALKBH7 could function as the wild-type protein.

DISCUSSION

The nonheme Fe(II)- and α-KG-dependent dioxygenases catalyze a wide range of oxidative reactions. Among them, AlkB family members, which mediate the oxidative DNA/RNA repair, are extensively studied both functionally and structurally. The function and substrate selection mechanisms of AlkB family members as nucleic acid oxygenase are clear because of their solved structures. They use Fe(II) to activate the dioxygen molecule for oxidation of the aberrant alkyl groups. A conserved nucleotide recognition lid covering the DSBH creates a cavity for modified nucleobase binding. This nucleotide recognition lid is also involved in the interaction with the phosphate backbone of nucleic acids. The minor β-sheet of DSBH plus several loops form the positively charged DNA/RNA binding groove. Although AlkB family members are mainly known as nucleic acid oxygenase in the past decade, several recent studies extend their function. ALKBH1 was reported to demethylate histone H2A (40), and ALKBH4 was shown to mediate demethylation of a monomethylated site (K84me1) in actin (41).

ALKBH7 is required for alkylation- and oxidation-induced programmed necrosis (7). It is unique because the ALKBH7-depleted cells are more resistant to DNA damage caused by alkylating agents than normal cells. ALKBH7 plays a role totally different from the protective role of AlkB, ALKBH2, ALKBH3, and ALKBH8 upon exposure to DNA-damaging agents. To understand the unusual function mechanism of ALKBH7, we solved the structure of ALKBH7 in complex with Mn(II), α-KG, or NOG. The crystal structure of ALKBH7 exhibits several unique features compared with other AlkB family members.

First and foremost, the conserved nucleotide recognition lid of AlkB family members is absent in ALKBH7 (Fig. 6*A*). Without the essential nucleotide recognition lid, ALKBH7 displays a solvent-exposed active site incapable of positioning the modified nucleobase, which basically rules out the possibility that ALKBH7 functions as a nucleic acid oxygenase. The solvent-exposed active site may not only abolish the binding of a modified nucleobase but may also potentially promote promiscuous catalysis of α-KG oxidation in the absence of main substrates. Release of reactive oxygen species due to the uncoupled reaction is harmful in cells, and Leu-110 is hydroxylated because of this. Loss of the conserved α-KG c-1 carboxylate-binding asparagine in ALKBH7 (Figs. 2 and 5*A*) results in weaker binding affinity of α-KG, which may lower the uncoupled turnover of α-KG in adaptation to the solvent-exposed active site. Moreover, the hydrophobic nature of residues at the active site may reflect the tolerance of ALKBH7 to potential oxidative damage because they are less susceptible to oxidation. Second, ALKBH7 has a negatively charged surface in equivalent position with the nucleic acid binding groove of other AlkB family members (Fig. 6*E*). An additional loop between strands β9 (βVII) and β10 (βVIII) of ALKBH7 creates the outer wall of the minor β-sheet of DSBH (Fig. 6*D* and supplemental movie S1). Four acidic residues (Asp-182, Glu-183, Glu-184, and Glu-189) in this loop combining with Glu-150 and Glu-153 from the β6-β7 loop, Glu-156 from strand β7, and Glu-178 from strand β9 are responsible for the negatively charged surface of ALKBH7. Binding of nucleic acid would be impossible because of the charge repulsion between the phosphate backbone and ALKBH7. In addition, the cleft opening into the active site is also negatively charged because of Glu-62, Asp-64, and Asp-67 in α2-β3 loop and Glu-75 and Glu-77 in strand β3. The negatively charged surface of ALKBH7 indicates that it may interact with a positively charged molecule, such as the lysine/arginine-rich protein. Further studies are in urgently needed to uncover the substrates of ALKBH7 in programmed necrosis and fat metabolism.

Structural comparison of ALKBH7 and other Fe(II)- and α-KG-dependent dioxygenases reveals the potential role of ALKBH7 as a protein hydroxylase. The conformations of ALKBH7 and PHD2 are similar, and they all prefer hydrophobic residues in the active center. Hydroxylation of either Pro-402 or Pro-564 in human HIF-1α by PHD2 enables human HIF-1α binding to the von Hippel-Lindau protein (49, 50). Hydroxylation of the target protein by ALKBH7 may enable its binding to the downstream elements and trigger the collapse of mitochondrial membrane potential. As a trigger of cell death, the interaction between ALKBH7 and its target protein and the hydroxylation reaction must be strictly controlled. No high confidence interaction partners of ALKBH7 was found by yeast two-hybrid screens (52), and the absence of stimulus might be the reason. CypD is a mitochondrial member of the cyclophilin family of peptidylprolyl cis-trans isomerases and has a crucial role in the mitochondrial permeability transition. CypD-deficient cells died normally in response to various apoptotic stimuli but showed resistance to necrotic cell death (53), and deletion of CypD in mice caused an abnormal accumulation of white adipose tissue resulting in obesity (54). These similar phenotypes of CypD and ALKBH7 indicate a potential relationship between them.

In summary, we solved the unique atomic resolution structures of ALKBH7 with a solvent-exposed active site and negatively charged surface. These features exclude the possibility that ALKBH7 functions as a nucleic acid oxygenase and indicate that ALKBH7 may interact with a positively charged molecule. The substrate of ALKBH7 may be peptides or proteins containing proline and lysine/arginine.

Our results point the way for future studies to address the signaling mechanism of the alkylation- and oxidation-induced programmed necrosis. The structure of ALKBH7 can also be exploited for the development of selective inhibitors to avoid unwarranted cell death in wounded or sick patients. Moreover, it also offers a foundation for drug design in treating metabolic diseases in humans and increasing the body weight of animals in livestock.

Acknowledgments—We thank Prof. Kazutake Tsujikawa and Prof. Jiemin Wong for cDNAs and discussion.

REFERENCES

1. Kroemer, G., Galluzzi, L., Vandenabeele, P., Abrams, J., Alnemri, E. S., Baehrecke, E. H., Blagosklonny, M. V., El-Deiry, W. S., Golstein, P., Green, D. R., Hengartner, M., Knight, R. A., Kumar, S., Lipton, S. A., Malorni, W., Nuñez, G., Peter, M. E., Tschopp, J., Yuan, J., Piacentini, M., Zhivotovsky,

B., Melino, G., and Nomenclature Committee on Cell Death 2009 (2009) Classification of cell death: recommendations of the Nomenclature Committee on Cell Death 2009. *Cell Death. Differ.* **16,** 3–11
2. Dunai, Z., Bauer, P. I., and Mihalik, R. (2011) Necroptosis: biochemical, physiological and pathological aspects. *Pathol. Oncol. Res.* **17,** 791–800
3. Ha, H. C., and Snyder, S. H. (1999) Poly(ADP-ribose) polymerase is a mediator of necrotic cell death by ATP depletion. *Proc. Natl. Acad. Sci. U.S.A.* **96,** 13978–13982
4. Cipriani, G., Rapizzi, E., Vannacci, A., Rizzuto, R., Moroni, F., and Chiarugi, A. (2005) Nuclear poly(ADP-ribose) polymerase-1 rapidly triggers mitochondrial dysfunction. *J. Biol. Chem.* **280,** 17227–17234
5. Alano, C. C., Garnier, P., Ying, W., Higashi, Y., Kauppinen, T. M., and Swanson, R. A. (2010) NAD^+ depletion is necessary and sufficient for poly(ADP-ribose) polymerase-1-mediated neuronal death. *J. Neurosci.* **30,** 2967–2978
6. Kreuzaler, P., and Watson, C. J. (2012) Killing a cancer: what are the alternatives? *Nat. Rev. Cancer* **12,** 411–424
7. Fu, D., Jordan, J. J., and Samson, L. D. (2013) Human ALKBH7 is required for alkylation- and oxidation-induced programmed necrosis. *Gene Dev.* **27,** 1089–1100
8. Solberg, A., Robertson, A. B., Aronsen, J. M., Rognmo, Ø., Sjaastad, I., Wisløff, U., and Klungland, A. (2013) Deletion of mouse Alkbh7 leads to obesity. *J. Mol. Cell Biol.* **5,** 194–203
9. Kurowski, M. A., Bhagwat, A. S., Papaj, G., and Bujnicki, J. M. (2003) Phylogenomic identification of five new human homologs of the DNA repair enzyme AlkB. *BMC Genomics* **4,** 48
10. Sanchez-Pulido, L., and Andrade-Navarro, M. A. (2007) The FTO (fat mass and obesity associated) gene codes for a novel member of the nonheme dioxygenase superfamily. *BMC Biochem.* **8,** 23
11. Loenarz, C., and Schofield, C. J. (2011) Physiological and biochemical aspects of hydroxylations and demethylations catalyzed by human 2-oxoglutarate oxygenases. *Trends Biochem. Sci.* **36,** 7–18
12. Falnes, P. Ø., Johansen, R. F., and Seeberg, E. (2002) AlkB-mediated oxidative demethylation reverses DNA damage in *Escherichia coli*. *Nature* **419,** 178–182
13. Delaney, J. C., and Essigmann, J. M. (2004) Mutagenesis, genotoxicity, and repair of 1-methyladenine, 3-alkylcytosines, 1-methylguanine, and 3-methylthymine in alkB *Escherichia coli*. *Proc. Natl. Acad. Sci. U.S.A.* **101,** 14051–14056
14. Delaney, J. C., Smeester, L., Wong, C., Frick, L. E., Taghizadeh, K., Wishnok, J. S., Drennan, C. L., Samson, L. D., and Essigmann, J. M. (2005) AlkB reverses etheno DNA lesions caused by lipid oxidation *in vitro* and *in vivo*. *Nat. Struct. Mol. Biol.* **12,** 855–860
15. Westbye, M. P., Feyzi, E., Aas, P. A., Vågbø, C. B., Talstad, V. A., Kavli, B., Hagen, L., Sundheim, O., Akbari, M., Liabakk, N. B., Slupphaug, G., Otterlei, M., and Krokan, H. E. (2008) Human AlkB homolog 1 is a mitochondrial protein that demethylates 3-methylcytosine in DNA and RNA. *J. Biol. Chem.* **283,** 25046–25056
16. Müller, T. A., Meek, K., and Hausinger, R. P. (2010) Human AlkB homologue 1 (ABH1) exhibits DNA lyase activity at abasic sites. *DNA Repair* **9,** 58–65
17. Duncan, T., Trewick, S. C., Koivisto, P., Bates, P. A., Lindahl, T., and Sedgwick, B. (2002) Reversal of DNA alkylation damage by two human dioxygenases. *Proc. Natl. Acad. Sci. U.S.A.* **99,** 16660–16665
18. Monsen, V. T., Sundheim, O., Aas, P. A., Westbye, M. P., Sousa, M. M., Slupphaug, G., and Krokan, H. E. (2010) Divergent ss-hairpins determine double-strand *versus* single-strand substrate recognition of human AlkB-homologues 2 and 3. *Nucleic Acids Res.* **38,** 6447–6455
19. Sundheim, O., Vågbø, C. B., Bjørås, M., Sousa, M. M., Talstad, V., Aas, P. A., Drabløs, F., Krokan, H. E., Tainer, J. A., and Slupphaug, G. (2006) Human ABH3 structure and key residues for oxidative demethylation to reverse DNA/RNA damage. *EMBO J.* **25,** 3389–3397
20. Yang, C. G., Yi, C., Duguid, E. M., Sullivan, C. T., Jian, X., Rice, P. A., and He, C. (2008) Crystal structures of DNA/RNA repair enzymes AlkB and ABH2 bound to dsDNA. *Nature* **452,** 961–965
21. Jia, G., Fu, Y., Zhao, X., Dai, Q., Zheng, G., Yang, Y., Yi, C., Lindahl, T., Pan, T., Yang, Y. G., and He, C. (2011) *N*6-Methyladenosine in nuclear RNA is a major substrate of the obesity-associated FTO. *Nat. Chem. Biol.* **7,** 885–887
22. Zheng, G., Dahl, J. A., Niu, Y., Fedorcsak, P., Huang, C. M., Li, C. J., Vågbø, C. B., Shi, Y., Wang, W. L., Song, S. H., Lu, Z., Bosmans, R. P., Dai, Q., Hao, Y. J., Yang, X., Zhao, W. M., Tong, W. M., Wang, X. J., Bogdan, F., Furu, K., Fu, Y., Jia, G., Zhao, X., Liu, J., Krokan, H. E., Klungland, A., Yang, Y. G., and He, C. (2013) ALKBH5 is a mammalian RNA demethylase that impacts RNA metabolism and mouse fertility. *Mol. Cell* **49,** 18–29
23. Fu, Y., Dai, Q., Zhang, W., Ren, J., Pan, T., and He, C. (2010) The AlkB domain of mammalian ABH8 catalyzes hydroxylation of 5-methoxycarbonylmethyluridine at the wobble position of tRNA. *Angew. Chem. Int. Ed. Engl.* **49,** 8885–8888
24. Lee, D. H., Jin, S. G., Cai, S., Chen, Y., Pfeifer, G. P., and O'Connor, T. R. (2005) Repair of methylation damage in DNA and RNA by mammalian AlkB homologues. *J. Biol. Chem.* **280,** 39448–39459
25. Ringvoll, J., Nordstrand, L. M., Vågbø, C. B., Talstad, V., Reite, K., Aas, P. A., Lauritzen, K. H., Liabakk, N. B., Bjørk, A., Doughty, R. W., Falnes, P. Ø., Krokan, H. E., and Klungland, A. (2006) Repair deficient mice reveal mABH2 as the primary oxidative demethylase for repairing 1meA and 3meC lesions in DNA. *EMBO J.* **25,** 2189–2198
26. Johannessen, T. C., Prestegarden, L., Grudic, A., Hegi, M. E., Tysnes, B. B., and Bjerkvig, R. (2013) The DNA repair protein ALKBH2 mediates temozolomide resistance in human glioblastoma cells. *Neuro-oncology* **15,** 269–278
27. Dango, S., Mosammaparast, N., Sowa, M. E., Xiong, L. J., Wu, F., Park, K., Rubin, M., Gygi, S., Harper, J. W., and Shi, Y. (2011) DNA unwinding by ASCC3 helicase is coupled to ALKBH3-dependent DNA alkylation repair and cancer cell proliferation. *Mol. Cell* **44,** 373–384
28. Fu, D., Brophy, J. A., Chan, C. T., Atmore, K. A., Begley, U., Paules, R. S., Dedon, P. C., Begley, T. J., and Samson, L. D. (2010) Human AlkB homolog ABH8 is a tRNA methyltransferase required for wobble uridine modification and DNA damage survival. *Mol. Cell. Biol.* **30,** 2449–2459
29. Fischer, J., Koch, L., Emmerling, C., Vierkotten, J., Peters, T., Brüning, J. C., and Rüther, U. (2009) Inactivation of the Fto gene protects from obesity. *Nature* **458,** 894–898
30. Wang, J., Kamtekar, S., Berman, A. J., and Steitz, T. A. (2005) Correction of x-ray intensities from single crystals containing lattice-translocation defects. *Acta Crystallogr. D Biol. Crystallogr.* **61,** 67–74
31. Otwinowski, Z., and Minor, W. (1997) in *Methods of Enzymology*(Carter, C. W., Jr., ed) pp. 307–326, Academic Press
32. Terwilliger, T. C., and Berendzen, J. (1999) Automated MAD and MIR structure solution. *Acta Crystallogr. D Biol. Crystallogr.* **55,** 849–861
33. Emsley, P., Lohkamp, B., Scott, W. G., and Cowtan, K. (2010) Features and development of Coot. *Acta Crystallogr. D Biol. Crystallogr.* **66,** 486–501
34. Murshudov, G. N., Skubák, P., Lebedev, A. A., Pannu, N. S., Steiner, R. A., Nicholls, R. A., Winn, M. D., Long, F., and Vagin, A. A. (2011) REFMAC5 for the refinement of macromolecular crystal structures. *Acta Crystallogr. D Biol. Crystallogr.* **67,** 355–367
35. Schrödinger, L. (2010) *The PyMOL Molecular Graphics System,* Version 1.3, Schrödinger, LLC, New York
36. McDonough, M. A., Loenarz, C., Chowdhury, R., Clifton, I. J., and Schofield, C. J. (2010) Structural studies on human 2-oxoglutarate dependent oxygenases. *Curr. Opin. Struct. Biol.* **20,** 659–672
37. Aik, W., McDonough, M. A., Thalhammer, A., Chowdhury, R., and Schofield, C. J. (2012) Role of the jelly-roll fold in substrate binding by 2-oxoglutarate oxygenases. *Curr. Opin. Struct. Biol.* **22,** 691–700
38. Aik, W., Scotti, J. S., Choi, H., Gong, L., Demetriades, M., Schofield, C. J., and McDonough, M. A. (2014) Structure of human RNA *N*(6)-methyladenine demethylase ALKBH5 provides insights into its mechanisms of nucleic acid recognition and demethylation. *Nucleic Acids Res.* **42,** 4741–4754
39. McDonough, M. A., Li, V., Flashman, E., Chowdhury, R., Mohr, C., Liénard, B. M., Zondlo, J., Oldham, N. J., Clifton, I. J., Lewis, J., McNeill, L. A., Kurzeja, R. J., Hewitson, K. S., Yang, E., Jordan, S., Syed, R. S., and Schofield, C. J. (2006) Cellular oxygen sensing: crystal structure of hypoxia-inducible factor prolyl hydroxylase (PHD2). *Proc. Natl. Acad. Sci. U.S.A.* **103,** 9814–9819
40. Ougland, R., Lando, D., Jonson, I., Dahl, J. A., Moen, M. N., Nordstrand, L. M., Rognes, T., Lee, J. T., Klungland, A., Kouzarides, T., and Larsen, E.

(2012) ALKBH1 is a histone H2A dioxygenase involved in neural differentiation. *Stem Cells* **30,** 2672–2682
41. Li, M. M., Nilsen, A., Shi, Y., Fusser, M., Ding, Y. H., Fu, Y., Liu, B., Niu, Y., Wu, Y. S., Huang, C. M., Olofsson, M., Jin, K. X., Lv, Y., Xu, X. Z., He, C., Dong, M. Q., Rendtlew Danielsen, J. M., Klungland, A., and Yang, Y. G. (2013) ALKBH4-dependent demethylation of actin regulates actomyosin dynamics. *Nat. Commun.* **4,** 1832
42. Yu, B., Edstrom, W. C., Benach, J., Hamuro, Y., Weber, P. C., Gibney, B. R., and Hunt, J. F. (2006) Crystal structures of catalytic complexes of the oxidative DNA/RNA repair enzyme AlkB. *Nature* **439,** 879–884
43. Han, Z., Niu, T., Chang, J., Lei, X., Zhao, M., Wang, Q., Cheng, W., Wang, J., Feng, Y., and Chai, J. (2010) Crystal structure of the FTO protein reveals basis for its substrate specificity. *Nature* **464,** 1205–1209
44. Feng, C., Liu, Y., Wang, G., Deng, Z., Zhang, Q., Wu, W., Tong, Y., Cheng, C., and Chen, Z. (2014) Crystal structures of the human RNA demethylase Alkbh5 reveal basis for substrate recognition. *J. Biol. Chem.* **289,** 11571–11583
45. Holland, P. J., and Hollis, T. (2010) Structural and mutational analysis of *Escherichia coli* AlkB provides insight into substrate specificity and DNA damage searching. *PLoS ONE* **5,** e8680
46. Pastore, C., Topalidou, I., Forouhar, F., Yan, A. C., Levy, M., and Hunt, J. F. (2012) Crystal structure and RNA binding properties of the RNA recognition motif (RRM) and AlkB domains in human AlkB homolog 8 (ABH8), an enzyme catalyzing tRNA hypermodification. *J. Biol. Chem.* **287,** 2130–2143
47. Holm, L., and Rosenström, P. (2010) Dali server: conservation mapping in 3D. *Nucleic Acids Res.* **38,** W545–W549
48. Chowdhury, R., McDonough, M. A., Mecinović, J., Loenarz, C., Flashman, E., Hewitson, K. S., Domene, C., and Schofield, C. J. (2009) Structural basis for binding of hypoxia-inducible factor to the oxygen-sensing prolyl hydroxylases. *Structure* **17,** 981–989
49. Bruick, R. K., and McKnight, S. L. (2001) A conserved family of prolyl-4-hydroxylases that modify HIF. *Science* **294,** 1337–1340
50. Epstein, A. C., Gleadle, J. M., McNeill, L. A., Hewitson, K. S., O'Rourke, J., Mole, D. R., Mukherji, M., Metzen, E., Wilson, M. I., Dhanda, A., Tian, Y. M., Masson, N., Hamilton, D. L., Jaakkola, P., Barstead, R., Hodgkin, J., Maxwell, P. H., Pugh, C. W., Schofield, C. J., and Ratcliffe, P. J. (2001) *C. elegans* EGL-9 and mammalian homologs define a family of dioxygenases that regulate HIF by prolyl hydroxylation. *Cell* **107,** 43–54
51. Mantri, M., Zhang, Z., McDonough, M. A., and Schofield, C. J. (2012) Autocatalysed oxidative modifications to 2-oxoglutarate-dependent oxygenases. *FEBS J.* **279,** 1563–1575
52. Bjørnstad, L. G., Meza, T. J., Otterlei, M., Olafsrud, S. M., Meza-Zepeda, L. A., and Falnes, P. Ø. (2012) Human ALKBH4 interacts with proteins associated with transcription. *PLoS One* **7,** e49045
53. Nakagawa, T., Shimizu, S., Watanabe, T., Yamaguchi, O., Otsu, K., Yamagata, H., Inohara, H., Kubo, T., and Tsujimoto, Y. (2005) Cyclophilin D-dependent mitochondrial permeability transition regulates some necrotic but not apoptotic cell death. *Nature* **434,** 652–658
54. Luvisetto, S., Basso, E., Petronilli, V., Bernardi, P., and Forte, M. (2008) Enhancement of anxiety, facilitation of avoidance behavior, and occurrence of adult-onset obesity in mice lacking mitochondrial cyclophilin D. *Neuroscience* **155,** 585–596